

Structure of the cooperative Xis–DNA complex reveals a micronucleoprotein filament that regulates phage lambda intasome assembly

Mohamad A. Abbani*, Christie V. Papagiannis†, My D. Sam*, Duilio Cascio*, Reid C. Johnson^{†‡§}, and Robert T. Clubb^{*‡§}

*Department of Chemistry and Biochemistry and University of California–Department of Energy Institute of Genomics and Proteomics, and †Molecular Biology Institute, University of California, 611 Charles Young Drive East, Los Angeles, CA 90095-1570; and ‡Department of Biological Chemistry, David Geffen School of Medicine, University of California, 10833 Le Conte Avenue, Los Angeles, CA 90095-1737

Edited by Kiyoshi Mizuuchi, National Institutes of Health, Bethesda, MD, and approved December 11, 2006 (received for review September 6, 2006)

The DNA architectural protein Xis regulates the construction of higher-order nucleoprotein intasomes that integrate and excise the genome of phage lambda from the *Escherichia coli* chromosome. Xis modulates the directionality of site-specific recombination by stimulating phage excision 10^6 -fold, while simultaneously inhibiting phage reintegration. Control is exerted by cooperatively assembling onto a ≈ 35 -bp DNA regulatory element, which it distorts to preferentially stabilize an excisive intasome. Here, we report the 2.6-Å crystal structure of the complex between three cooperatively bound Xis proteins and a 33-bp DNA containing the regulatory element. Xis binds DNA in a head-to-tail orientation to generate a micronucleoprotein filament. Although each protomer is anchored to the duplex by a similar set of nonbase specific contacts, malleable protein–DNA interactions enable binding to sites that differ in nucleotide sequence. Proteins at the ends of the duplex sequence specifically recognize similar binding sites and participate in cooperative binding via protein–protein interactions with a bridging Xis protomer that is bound in a less specific manner. Formation of this polymer introduces $\approx 72^\circ$ of curvature into the DNA with slight positive writhe, which functions to connect disparate segments of DNA bridged by integrase within the excisive intasome.

DNA bending | recombination directionality factors | site-specific DNA recombination | x-ray structure

Mobile genetic elements such as bacteriophages, conjugative transposons, and pathogenicity islands promote the lateral exchange of foreign DNA, enabling bacteria to acquire metabolic, pathogenic, and antibiotic resistance determinants. To prevent potentially catastrophic changes in the genome, these DNA rearrangements are often tightly controlled by regulatory factors that function together with the recombinase. The integration and excision reactions of phage λ , which are controlled by the phage-encoded Xis protein, serve as a paradigm for studies of regulated site-specific recombination (1). Upon infection, specific DNA attachment sites located on the circularized phage genome (*attP*) and bacterial chromosome (*attB*) recombine to generate the integrated prophage with flanking hybrid sites (*attL* and *attR*) (Fig. 1A). Cellular DNA damage initiates a series of events that result in prophage excision to regenerate *attP* on the episomal phage genome and *attB* on the chromosome. Although the DNA strand transfer steps in each reaction are catalyzed by the phage-encoded tyrosine recombinase integrase (Int) protein, and are mechanistically similar, directionality control is achieved by guiding the assembly of distinct higher-order nucleoprotein structures called intasomes. Viral integration occurs within an integrative intasome containing Int and the *Escherichia coli*-encoded integration host factor (IHF) (2, 3), whereas excision is performed within an alternative excisive intasome complex containing Int, Xis, IHF, and the factor for inversion stimulation (4–7).

Xis is the master regulator of λ recombination, stimulating phage excision *in vivo* $>10^6$ -fold, while simultaneously inhibiting phage

reintegration (8–10). These dual and opposing effects are elicited by its cooperative binding to a ≈ 35 -bp DNA segment that contains two conserved sequence elements, X1 and X2 (Fig. 1B). DNA bending by Xis promotes formation of the excisive intasome, but antagonizes formation of an integrative intasome (8, 11). In addition, Xis stabilizes the synaptic complex by directly interacting with Int bound to the arms of the phage. Previously, the NMR structure of Xis (12, 13) and the x-ray structure of the complex between a single Xis protein and DNA have been reported (14). Although this work revealed how Xis recognizes a single binding site, the mechanism through which it cooperatively binds and distorts the *attR* regulatory element has remained enigmatic. Here, we show that three Xis monomers work in concert to substantially bend DNA by forming a micronucleoprotein filament. The mechanistic implications of the structure on the site-specific recombination reactions of phage λ and the functions of recombination directionality factors in other systems are discussed.

Results and Discussion

Three Xis Proteins Cooperatively Bind to the *attR* Regulatory Element.

Traditionally, two Xis proteins have been thought to bind to two related 13-bp sequences called X1 and X2 (Fig. 1B). However, the small size of the Xis protein and the 7-bp separation between the X1 and X2 sites has made it difficult to envision how cooperative binding could be achieved. Moreover, the sites are arranged in a head-to-tail configuration that would appear to necessitate the formation of an unusual asymmetric protein–DNA complex. To determine the number of Xis proteins that bind the regulatory element, we performed EMSAs. As observed (8, 13), Xis forms a single low mobility complex over the Xis binding region embedded in a 263-bp fragment from *attR* (Fig. 2A). As this DNA fragment contains at least two binding sites for Xis, the results suggest that binding is highly cooperative. Unexpectedly, we find that cooperative binding by Xis is compromised on short DNA fragments. The gel in Fig. 2B reveals three distinct Xis-dependent bands over a broad range of Xis levels on a 54-bp fragment covering the Xis binding region [see supporting information (SI) Fig. 6]. The number

Author contributions: M.A.A., C.V.P., and M.D.S. contributed equally to this work; M.A.A., C.V.P., M.D.S., R.C.J., and R.T.C. designed research; M.A.A., C.V.P., M.D.S., and D.C. performed research; M.A.A., C.V.P., D.C., R.C.J., and R.T.C. analyzed data; and M.A.A., C.V.P., R.C.J., and R.T.C. wrote the paper.

The authors declare no conflict of interest.

This article is a PNAS direct submission.

Abbreviations: Int, integrase; BS³, bis(sulfosuccinimidyl)suberatel; DSG, disuccinimidyl glutarate.

Data deposition: The atomic coordinates have been deposited in the Protein Data Bank, www.pdb.org (PDB ID code 2IEF).

§To whom correspondence may be addressed. E-mail: rcjohnson@mednet.ucla.edu or rclubb@mbi.ucla.edu.

This article contains supporting information online at www.pnas.org/cgi/content/full/0607820104/DC1.

© 2007 by The National Academy of Sciences of the USA

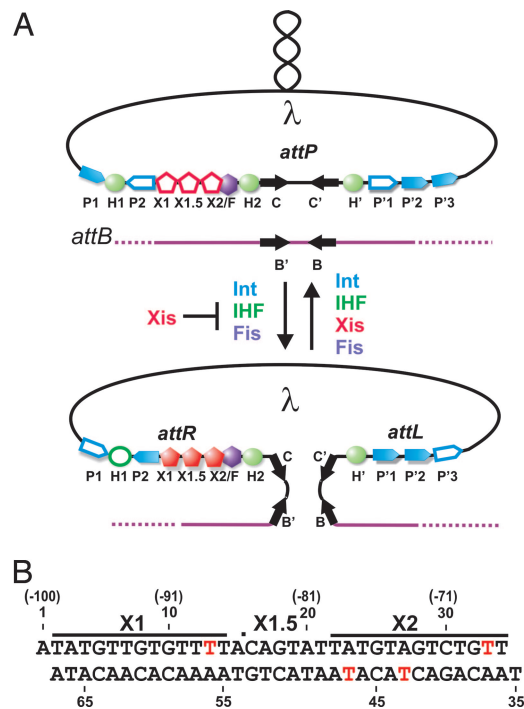


Fig. 1. Integrative and excisive recombination of phage λ . (A) Schematic representation of the phage λ site-specific recombination reactions. The supercoiled phage genome inserts into the *E. coli* chromosome by recombination between the *attP* (phage) and *attB* (bacterial) sites to generate the *attL* and *attR* sites that are substrates for excisive recombination. Proteins required for integration and excision are indicated: Int, integration host factor (IHF), and factor for inversion stimulation (Fis). Excise (Xis) is required for excision and inhibits integration. Filled symbols, binding sites used; open symbols, binding sites not used during the integration or excision reactions (1). (B) Xis binding sequence used to form crystals with red nucleotides depicting 5-bromo-uracil substitutions used for phasing. The dot between nucleotides 15 and 16 represents a nick in the DNA present after annealing the three oligonucleotides. The nucleotide numbers in parentheses are relative to the center of the *attR* core site, and the lines represent the conventional binding sites based on *in vitro* footprinting data and DNA sequence relationships (40).

of Xis proteins in the slowest mobility complex (labeled 3X in Fig. 2B) was addressed by using a fluorescein-labeled DNA fragment and ^{32}P -labeled Xis. The Xis used for this experiment had the C-terminal 17-aa residues that are disordered in solution replaced with a kinase tag ($^{\Delta 55}\text{Xis}^{\text{HMK}}$). We have shown previously that $^{\Delta 55}\text{Xis}$ binds *attR* in a cooperative manner that is nearly indistinguishable from the full-length protein (13). Quantifying the fluorescence and radioactivity in the complex gave a molar ratio of 3.6 ± 0.9 Xis molecules per DNA substrate. These experiments suggest that at least three Xis protomers are present in the *attR* regulatory complex.

Protein cross-linking experiments were performed to independently define the number of Xis protomers in the *attR* complex. ^{32}P -labeled full-length Xis^{HMK} or $^{\Delta 55}\text{Xis}^{\text{HMK}}$ were incubated with the fluorescein-labeled *attR* substrate and subjected to cross-linking with amine-specific cross-linkers. After purification of the Xis-DNA complexes on native gels, the cross-linked Xis molecules were displayed on SDS/PAGE. The complex that is predicted to contain two Xis protomers from the native gel (2X in Fig. 2B) contains a single product after cross-linking with bis(sulfosuccinimidyl)suberate (BS^3) (11-Å spacer) whose migration is consistent with two linked Xis monomers (Fig. 2C, lane 2), and the slowest mobility band on the native gel (3X in Fig. 2B) contains products consistent with cross-linked trimers and dimers (Fig. 2C, lane 3). The slow mobility complexes formed with $^{\Delta 55}\text{Xis}$ and cross-linked with BS^3

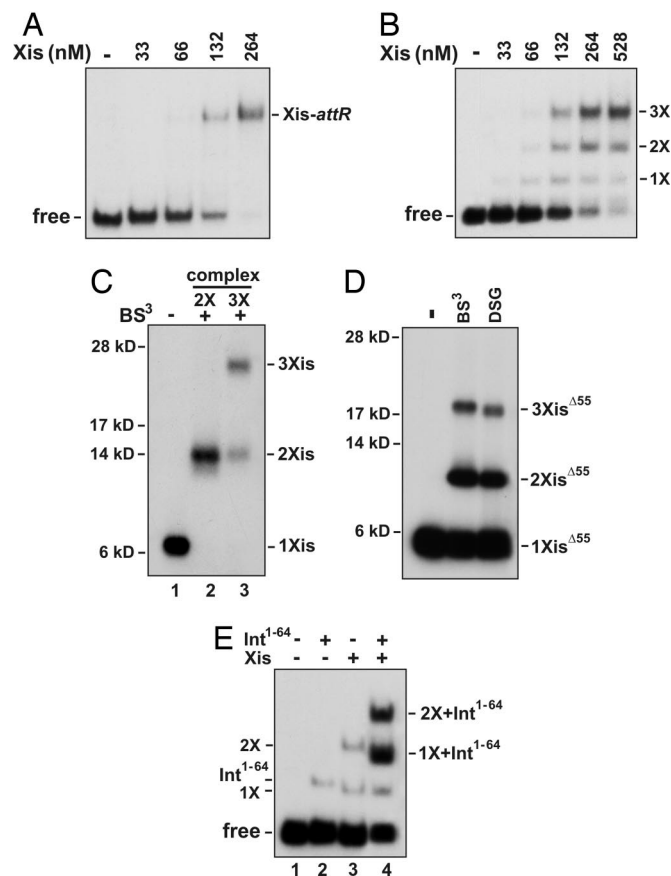


Fig. 2. A trimer of Xis cooperatively binds DNA. (A) Cooperative Xis binding to long *attR* DNA fragments. Increasing concentrations of Xis were incubated with a ^{32}P -labeled *attR* fragment (-220 to +43) and electrophoresed in a native polyacrylamide gel. (B) Xis binding to short *attR* DNA fragments (-104 to -51) exhibits reduced cooperativity. 1X, 2X, and 3X represent DNA complexes postulated to contain one, two, and three Xis monomers, respectively. (C) Cross-linking of Xis-*attR* complexes. ^{32}P -labeled Xis^{HMK} was incubated with fluorescein-labeled *attR* DNA (-104 to -54), subjected to cross-linking with BS^3 , and electrophoresed in a native gel as in B. Xis complexes representing 2X and 3X were extracted from the native gel and subjected to SDS/PAGE. The number of cross-linked Xis monomers in each product band is based on their apparent molecular mass. (D) Cross-linking of $^{\Delta 55}\text{Xis}$ -*attR* complexes. Protocol was the same as in C except that ^{32}P -labeled $^{\Delta 55}\text{Xis}^{\text{HMK}}$ was subjected to cross-linking with BS^3 (11-Å spacer) or DSG (8-Å spacer), and the cross-linked products were extracted from the dominant slowest migrating complex. (E) Binding of Int¹⁻⁶⁴ and two Xis protomers to *attR* fragments missing the X2 site. Xis (0.53 μM) and HisInt¹⁻⁶⁴ (3 μM) were incubated with a ^{32}P -labeled 45-bp probe (-121 to -77) containing the P2 and X1 binding sites as designated and electrophoresed in a native polyacrylamide gel. The identities of each of the bands based on their electrophoretic mobilities are denoted. The sequences of the oligonucleotide substrates are given in SI Fig. 6.

or disuccinimidyl glutarate (DSG) (8-Å spacer) also contained linked trimer and dimer products (Fig. 2D). The less efficient cross-linking obtained with $^{\Delta 55}\text{Xis}$ compared with that of full-length Xis probably reflects the absence of the lysine-rich and unstructured C terminus on the truncated derivative. Combined, the cross-linking and EMSA stoichiometry data indicate that three proximally positioned Xis proteins cooperatively bind the *attR* regulatory element.

EMSA experiments using truncated *attR* DNA segments suggest that the third Xis protomer binds between the X1 and X2 sites. In Fig. 2E, the DNA probe contained the P2 Int binding site and sequences over the Xis regulatory unit up to the beginning of the X2 sequence (-121 to -77) (SI Fig. 6). For this experiment we also

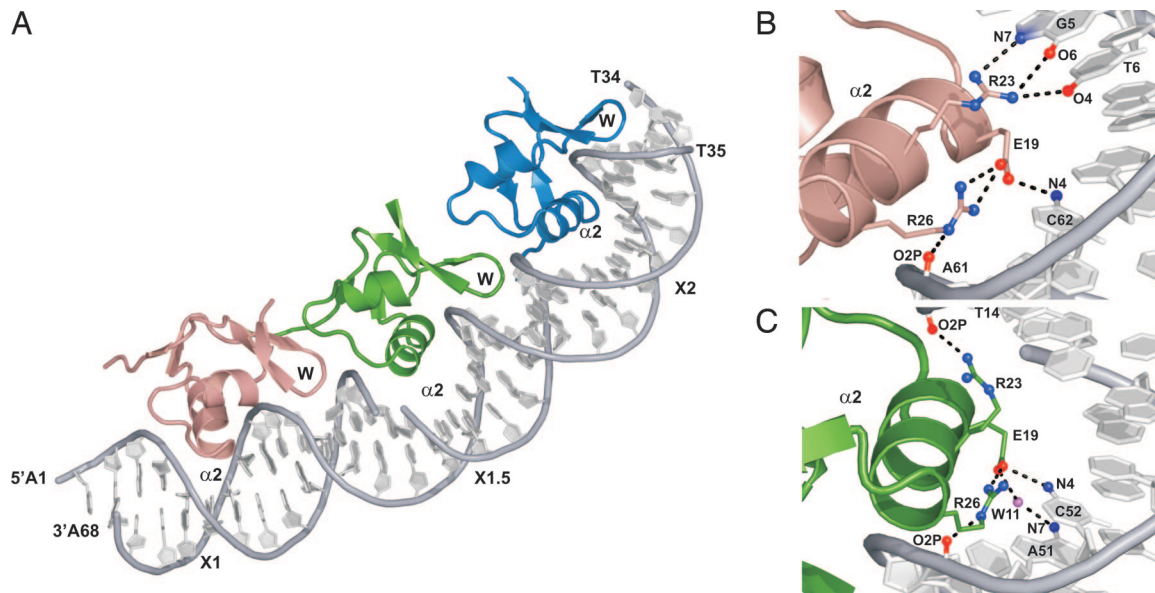


Fig. 3. The structural basis of cooperative binding is revealed by crystallography. (A) X-ray crystal structure of Xis bound to the Xis binding region. Xis monomers bound to the X1, X1.5, and X2 sites are colored dark salmon, green, and blue, respectively. The nick present in the top strand of the DNA duplex is a result of annealing three complementary DNA strands (Fig. 1B). The proteins adopt nearly identical “winged” helix structures (the backbone coordinates of residues Tyr-2–Val-50 in each protomer can be superimposed with a rmsd of 0.22 Å). The secondary structural elements in this fold are arranged in the following configuration: β 1- α 1-L- α 2-B1- β 2- β 3-W- β 4-B2- β 5, where L, W, and B are the loop, wing, and bulge structures, respectively. Residues within each secondary structural element are as follows: β 1 (Tyr-2–Thr-4), α 1 (Leu-5–Arg-11), L (Gln-12–Ser-17), α 2 (Leu-18–Arg-26), B1 (Glu-27–Arg-29), β 2 (Ile-30–Phe-31), β 3 (Val-35–Asp-37), W (Gly-38–Arg-39), β 4 (Glu-40–His-44), B2 (Glu-45–Ala-47), and β 5 (Val-48–Lys-49). (B and C) Residues within Xis–DNA interfaces involved in hydrogen bonding. (B) Shown is the interface between DNA and the Xis monomer bound at X1. (C) Shown is the interface between DNA and the Xis monomer bound at X1.5.

used the N-terminal His-tagged domain of Int (HisInt^{1-64}) that contains the DNA-binding and Xis cooperativity determinants (15–17). As shown in lane 2 of Fig. 2E, a weak complex is formed in the presence of HisInt^{1-64} alone, which corresponds to a monomer of HisInt^{1-64} bound to P2. In the absence of HisInt^{1-64} , WT Xis forms two weak complexes on this substrate (Fig. 2E, lane 3), whereas addition of both Xis and HisInt^{1-64} results in the formation of two prominent novel complexes (Fig. 2E, lane 4). The migration of the faster band is consistent with the presence of one Xis monomer and one HisInt^{1-64} monomer, whereas the slower migrating band is consistent with the presence of two Xis monomers and one HisInt^{1-64} monomer. This result supports a model in which Xis bound to X1 recruits an additional Xis protomer in the presence of Int, even though the X2 site is missing from the probe, and strongly implies that in the trimeric Xis–DNA complex, sites X1 and X2, and the intervening DNA, are occupied by Xis.

The Structure of Three Xis Proteins Bound to the X1–X2 DNA Segment Reveals a Micronucleoprotein Filament. To gain a high-resolution view of the cooperative Xis–DNA complex, we solved the cocrystal structure of Δ^{55} Xis bound to a 33-bp DNA duplex containing sites X1 and X2 (the Xis–DNA^{X1–X2} complex). The structure was refined to 2.6-Å with R_{work} and R_{free} values of 19.9% and 24.6%, respectively (SI Table 1). The asymmetric unit of the Xis–DNA^{X1–X2} complex contains three proteins bound to the DNA molecule. The complex resembles a nucleoprotein filament as the proteins are positioned in a head-to-tail arrangement along one face of the duplex forming a continuous interface that buries 5,100 Å² of solvent-exposed surface area (Fig. 3A). The proteins adopt nearly identical “winged” helix structures that are very similar to the structure of Xis in the DNA free state and its conformation when bound to a single DNA binding site (described in Fig. 3A legend). However, in this complex, unique protein–protein interactions function to cumulatively bend the duplex by $\approx 72^\circ$. A summary of the Xis–DNA contacts observed in the structure is presented in SI Fig. 7.

The three tandemly arranged proteins are positioned over their respective binding sites in a similar manner, with each inserting its α 2 helix and wing motif into the major and minor grooves, respectively. Base-specific recognition is primarily achieved by Xis interactions with the terminal X1 and X2 sites that share nearly identical nucleotide sequences. In contrast, the third protomer is bound in a largely nonspecific manner to a central site that differs substantially in nucleotide sequence, hereafter referred to as site X1.5. Sites X1 and X2 are recognized by major groove contacts from the side chains of Glu-19 and Arg-23 in the α 2 helix. At each interface, the side chain of Glu-19 forms a salt bridge with the guanidino group of Arg-26, which positions it to accept a hydrogen bond from the N4 amine of a conserved cytosine base (C42 and C62 in sites X1 and X2, respectively) (Fig. 3B). In addition, the guanidino group of Arg-23 donates hydrogen bonds to conserved G5–T6 (site X1) and G25–T26 (site X2) base steps. Locking the recognition helix into place is a network of contacts to the surrounding phosphodiester backbone that originate from residues within the turn preceding helix α 2, the β 3/ β 4 wing, and the recognition helix (SI Fig. 7). All of the nonspecific and specific interactions at sites X1 and X2 are compatible with extensive mutagenesis data describing the Xis–DNA interaction (13, 18). Moreover, DNA regions protected from hydroxyl radical cleavage by Xis binding to long (203 bp) DNA fragments in solution correspond well to the locations of the Xis wings at all three binding sites in the crystal (SI Fig. 8).

In the crystal structure, pliant interfacial side chains enable Xis to nonspecifically bind the central X1.5 site. In the major groove of site X1.5, an A–C base step replaces the conserved G–T base step that is sequence-specifically recognized in sites X1 and X2. To accommodate this alteration, the side chain of Arg-23 is rotated away from the major groove to form a salt bridge with the phosphate of T14 (Fig. 3C). Interestingly, Arg-23 can readily toggle between specific and nonspecific binding conformations, because model building of the electron density at site X2 reveals that it contacts the G–T base step only $\approx 25\%$ of the time in the crystal,

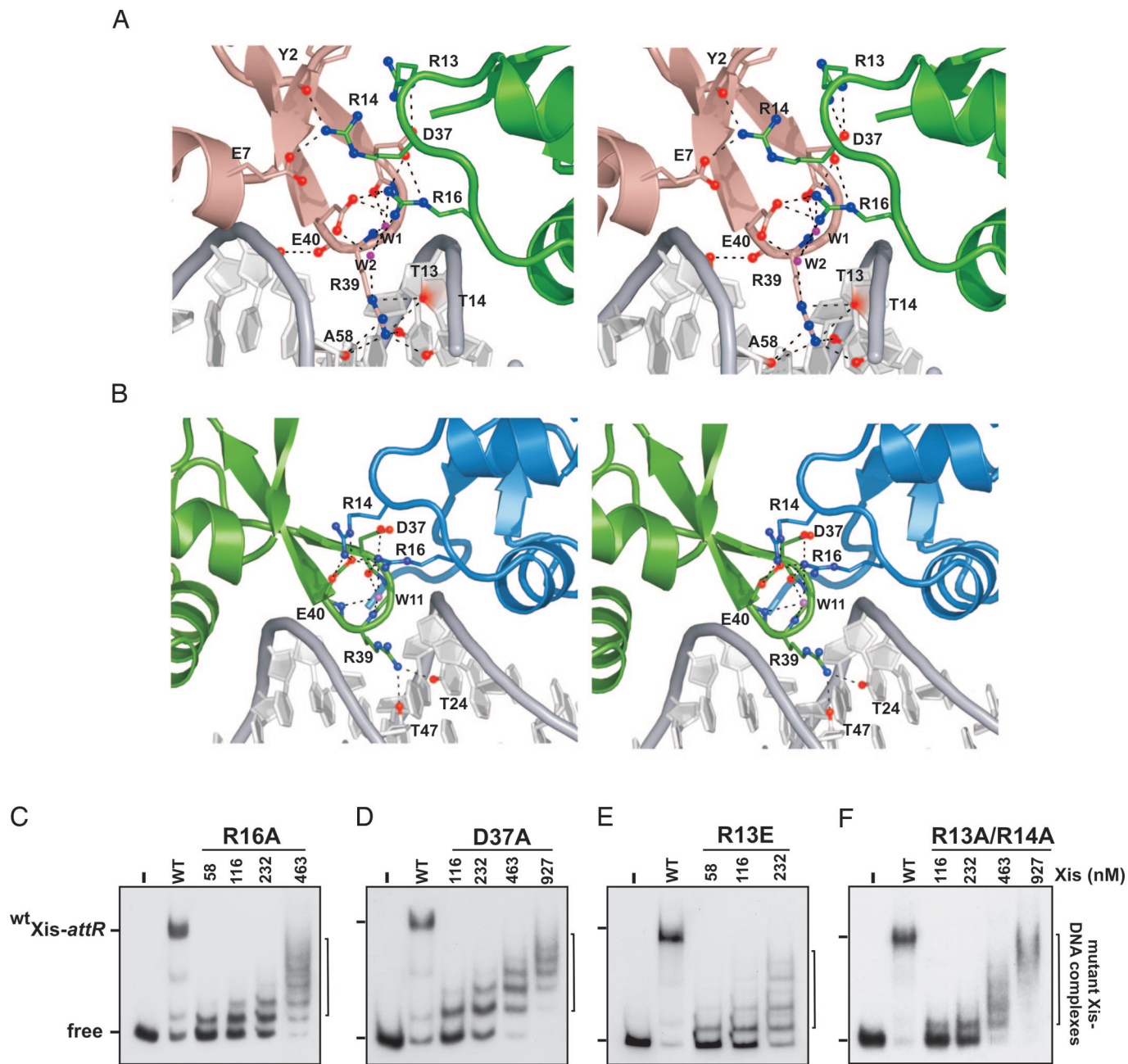


Fig. 4. Protein-protein interactions stabilize a nucleoprotein filament. (A and B) Cross-eyed stereoviews of residues within Xis-Xis interfaces involved in hydrogen bonding or ionic interactions in the Xis cooperative complex. (A) The interface between the Xis monomers bound at X1 (dark salmon) and X1.5 (green). (B) The interface between Xis monomers bound at X1.5 (green) and X2 (blue). (C–F) The effects of mutations in the Xis protein interfaces. Each panel shows a titration of the Xis mutant on the 263 *attR* fragment (–220 to +43) used in Fig. 2A. The identity of the Xis mutant is indicated at the top: R16A (C), D37A (D), R13E (E), and a double R13A and R14A mutant (F). The lanes designated WT contained reactions using 116 nM WT Xis; – designates that no Xis was added. Data shown for the R16A mutant are modified from figure 5C of ref. 13.

whereas the rest of the time it adopts the phosphate contacting conformation observed at site X1.5. Structural plasticity in the protein–DNA interface extends into the minor groove where contacts primarily originate from the side chain of Arg-39 located in the wing. Hydrogen bonds to the O2 atoms of T14, T24, and T34 are conserved at all three sites, but additional hydrogen bonds to thymines and adenines are formed at each site, depending on the sequence. Although radical changes in the nucleotide sequence of X1.5 can be made without adversely affecting filament formation (data not shown), the DNA sequence within X1.5 contains an appropriately positioned cytosine base that enables a lone sequence-specific contact from the side chain of Glu-19 (Fig. 3C).

Malleable Xis–Xis Interactions Promote Cooperative Filament Assembly and DNA Bending. Cooperative binding is mediated by the Xis protein bound to site X1.5, which contains two protein-binding surfaces that participate in reciprocal interactions with adjacent protomers. It uses residues within the turn that connects helices $\alpha 1$ and $\alpha 2$ (the $\alpha 1$ – $\alpha 2$ turn) to contact the wing of the protomer bound to site X1 (Fig. 4A; X1–X1.5 interface), whereas residues within its wing contact the $\alpha 1$ – $\alpha 2$ turn of Xis bound at site X2 (Fig. 4B; X1.5–X2 interface). Electrostatic interactions predominate within each interface and exclude a similar amount of solvent accessible surface area (the X1–X1.5 and X1.5–X2 interfaces bury 700 and

600 Å, respectively). Although similar sets of amino acids are involved, the interprotomer interactions at each interface are strikingly different, because the protomers bound to sites X1–X1.5 are rotated with respect to one another by 15°, whereas those bound at the X1.5–X2 interface are positioned at a 31° angle. As a result, only a single set of hydrogen bonding and electrostatic contacts are conserved within each interface; the side chain of Arg-16 originating from the $\alpha 1$ – $\alpha 2$ turn contacts the carboxyl side chains of Asp-37 and Glu-40 in the neighboring protomer (Fig. 4*A* and *B*). Consistent with the importance of these interactions implied by the structure, mutants containing alanine substitutions at either Arg-16 and Asp-37 no longer cooperatively bind DNA and only form nonspecific complexes (Fig. 4*C* and *D*) (13). In addition, an Xis protein containing a Glu-40–Ala mutation has been reported to exhibit increased nonspecific binding (18).

The remaining interprotomer interactions are unique, but generally involve the same amino acids. For example, in both interfaces the side chain of Arg-14 interacts with residues in an adjacent protomer. When it is located in the X2-bound Xis protein, Arg-14 forms a salt bridge to the Glu-40 side chain of Xis bound to site X1.5. In contrast, when Arg-14 originates from the X1.5-bound protomer, it contacts the side chain of Glu-7 and backbone atoms of the protein at site X1. The side chain of Arg-13 is involved in direct interactions only at the X1–X1.5 interface, where it is positioned to form multiple contacts with Asp-37. These interactions appear to play a less important role in stabilizing the complex because R13A and R14A mutants of Xis have comparatively milder binding phenotypes as compared with alanine mutants that alter Arg-16 and Asp-37 (data not shown). However, single R13E (Fig. 4*E*) and double R13A, R14A (Fig. 4*F*) mutants exhibit severe reductions in cooperative binding, demonstrating that these residues also participate in stabilizing the *attR* complex. Related, but nonidentical, contacts between interfaces within protein filaments that polymerize on DNA have been observed previously (e.g., refs. 19 and 20).

Although Xis only modestly distorts DNA when bound to a single site (14), interprotomer interactions within the filament stabilize in-phase DNA distortions that cumulatively bend the duplex by 72°. At each binding site a series of modest positive roll angle changes in base steps proximal to the recognition helix narrows the major groove by as much as 2.5 Å (8.5 Å in the complex versus 11 Å in typical B-form DNA). Further bending toward the protein occurs at the adjacent minor groove interfaces, which are also compacted to accommodate insertion of Arg-39 for direct and water-mediated hydrogen bonding. Contacts from adjacent Xis protomers in the filament are required for maximal bending. At sites X1 and X1.5, which exhibit the largest degree of bending (38° and 24°, respectively), interactions originating from a downstream positioned Xis protomer facilitate minor groove compression by neutralizing anionic phosphates and stabilizing the positioning of the wing (Fig. 4*A* and *B*). The absence of these contacts at the terminal X2 interface and in a complex that contained a single Xis bound to DNA (14) may explain why the DNA in these structures is only modestly bent. Although there is a nick in the DNA used to form the crystal, a comparison of bending between sites X1 and X1.5, where the nick resides, indicates that its contribution to the overall bending of the DNA is minimal.

Models of the excisive intasome require Xis to juxtapose distally positioned Int arm- and core-binding sites by substantially altering the trajectory of DNA. The curvature introduced by the three contiguous Xis protomers in the Xis–DNA^{X1–X2} crystal structure demonstrates how Xis performs this critical architectural function. We attempted to dock the Xis–DNA^{X1–X2} crystal structure onto a recent structure of an Int tetramer bound to antiparallel discontinuous DNA segments representing the P and P' arm binding sites plus core binding sites in a Holliday junction configuration (21). The resulting connection of the P arm and core Int binding sites generated a structure for the intact excisive intasome that is

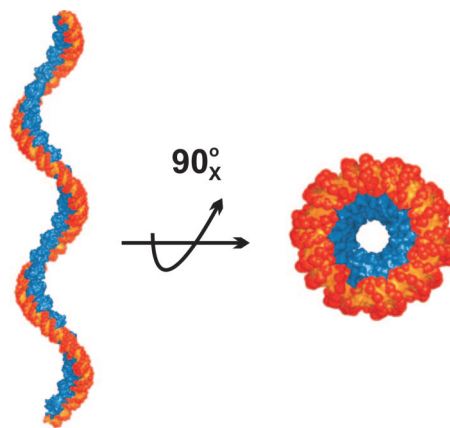


Fig. 5. Structure-based model of an extended Xis–DNA filament. Units of the Xis–DNA^{X1–X2} crystal structure were stacked end-to-end by superimposing site X1 over X1.5 to assemble a pseudo-continuous helix with a pitch of ≈ 22 nm. The model is shown perpendicular (*Left*) and parallel (*Right*) to the superhelical axis. Proteins are blue; DNA is orange and red.

incompatible with the previously established temporal order of DNA exchanges that occur during the excision reaction (22, 23). Thus, additional structural information with respect to the configuration of Int arm sites will be required to generate a structural model for the excisive intasome.

Nucleoprotein Filaments. Xis is the founding member of a diverse family of proteins that function to control reactions that rearrange DNA, called recombination directionality factors (RDFs) (24). Many of the RDFs share two common features with Xis: they adopt a similar winged-helix fold and cooperatively bind DNA as oligomers to produce extensive footprints (25–30). For example, the small Xis protein encoded by mycobacteriophage L5 is predicted to bind to four related sequence motifs spaced ≈ 10 bp apart to form a stable and bent DNA complex (27). The low molecular weight Xis protein from the Tn916 transposon also exhibits similar binding behavior and produces large footprints that contain hypersensitive cleavage sites characteristic of wrapped or bent DNA (31, 32). It seems likely that many of these proteins also assemble into nucleoprotein filaments, which function to stabilize recombinogenic higher-order structures. In the λ Xis microfilament, the bends introduced by each Xis protein are not coplanar, resulting in positive writhe that is readily visualized when an extended filament is modeled (Fig. 5). The DNA encircles the Xis protomers in the filament, possibly explaining why DNA bound by RDFs frequently exhibit periodic DNase I hypersensitivity.

Nucleoprotein filaments play important roles in other types of reactions. The most intensively studied filaments are those assembled by the RecA/RAD51 family of proteins, which catalyze homologous DNA pairing and strand exchange (33). Polymerization of DnaA within the *oriC* DNA region is believed to control open complex formation during initiation of replication (34). Formation of H-NS filaments containing one or two DNA duplex segments has been shown to silence transcription at promoters (35). In addition, localized filaments of nucleoid proteins are believed to contribute to compaction of bacterial chromosomes (36). Some of these protein filaments have been visualized by x-ray crystallography at varying resolutions [e.g., RecA (37), RAD51 (19), and DnaA (31)], but in most cases, the DNA was not present during crystal growth or not visible in the electron density maps. Although the details of the molecular interactions involved in each system will no doubt vary, the present structure of the Xis–DNA^{X1–X2} complex reveals how pliant protein–protein and protein–DNA interactions contribute to polymerization along DNA.

Materials and Methods

DNA Binding, Stoichiometry, and Cross-Linking Assays. Xis–DNA binding reactions and EMSAs using WT and mutant derivatives of Xis were performed as described (13). Full-length Xis^{HMK} contains the sequence coding for MRRASL added by PCR to the N terminus of otherwise WT Xis, and Δ^{55} Xis^{HMK} contains the sequence coding for ARRASL(TAA) added after residue 55 of Xis containing Cys-28 replaced with alanine. HisInt^{1–64} that was used in Fig. 2E contains the first 64 residues of Int with a six-histidine tag at the N terminus. DNA probes were generated by PCR where one or both primers were 5' ³²P-end-labeled; Fig. 2E shows a synthetic duplex oligonucleotide probe representing the *attR* sequence from –121 to –77 (SI Fig. 6). HPLC-purified fluorescein (6-FAM)-labeled 51-bp oligonucleotides representing the *attR* sequence between –104 to –54 (SI Fig. 6) were purchased from Sigma-Genosys (St. Louis, MO). Stoichiometry experiments using ³²P-labeled Δ^{55} Xis^{HMK} and the 6-FAM duplex oligonucleotides were performed essentially as described (38). Xis cross-linking reactions were performed in a similar manner to those described in ref. 39.

Binding reactions were assembled on the 6-FAM 51-bp *attR* oligonucleotides with 525 nM ³²P-labeled Xis^{HMK} or Δ^{55} Xis^{HMK}. The reactions were then incubated with 3.4 mM BS³ or DSG for 60 min at 37°C, quenched with the addition of 20 mM glycine, and applied to an 8% native polyacrylamide gel. Xis–DNA complexes were localized by fluorimaging and phosphorimaging, relevant bands were excised, and Xis proteins were recovered and subjected to SDS/PAGE following the protocols described (39).

Crystallization, Data Collection, and Structure Determination. Details describing complex crystallization, data collection, and structure determination are provided in SI Text. A representative portion of the experimental electron density map after solvent flattening is shown in SI Fig. 9.

We thank Michael Sawaya, Carlos Lopez, Corie Ralston, and the ALS beamline 8.2.2 staff for useful discussions. This work was supported by National Institutes of Health Grants GM57487 (to R.T.C.) and GM38509 (to R.C.J.).

1. Azaro MA, Landy A (2002) in *Mobile II*, eds Craig NL, Craigie R, Gellert M, Lambowitz AM (Am Soc Microbiol, Washington, DC), pp 118–148.
2. Miller HI, Kikuchi Y, Nash HA, Weisberg RA, Friedman DI (1979) *Cold Spring Harb Symp Quant Biol* 43:1121–1126.
3. Nash HA, Robertson CA (1981) *J Biol Chem* 256:9246–9253.
4. Abremski K, Gottesman S (1982) *J Biol Chem* 257:9658–9662.
5. Guarneros G, Echols H (1970) *J Mol Biol* 47:565–574.
6. Ball CA, Johnson RC (1991) *J Bacteriol* 173:4027–4031.
7. Thompson JF, Moitoso de Vargas L, Koch C, Kahmann R, Landy A (1987) *Cell* 50:901–908.
8. Bushman W, Yin S, Thio LL, Landy A (1984) *Cell* 39:699–706.
9. Franz B, Landy A (1995) *EMBO J* 14:397–406.
10. Moitoso de Vargas L, Landy A (1991) *Proc Natl Acad Sci USA* 88:588–592.
11. Thompson JF, Landy A (1988) *Nucleic Acids Res* 16:9687–9705.
12. Rogov VV, Lucke C, Muresanu L, Wienk H, Kleinhaus I, Werner K, Lohr F, Pristovsek P, Ruterjans H (2003) *Eur J Biochem* 270:4846–4858.
13. Sam MD, Papagiannis C, Connolly KM, Corselli L, Iwahara J, Lee J, Phillips M, Wojciak JM, Johnson RC, Clubb RT (2002) *J Mol Biol* 324:791–805.
14. Sam MD, Cascio D, Johnson RC, Clubb RT (2004) *J Mol Biol* 338:229–240.
15. Warren D, Sam MD, Manley K, Sarkar D, Lee SY, Abbani M, Wojciak JM, Clubb RT, Landy A (2003) *Proc Natl Acad Sci USA* 100:8176–8181.
16. Sarkar D, Azaro MA, Aihara H, Papagiannis CV, Tirumalai R, Nunes-Duby SE, Johnson RC, Ellenberger T, Landy A (2002) *J Mol Biol* 324:775–789.
17. Cho EH, Gumpport RI, Gardner JF (2002) *J Bacteriol* 184:5200–5203.
18. Cho EH, Alcaraz R, Jr, Gumpport RI, Gardner JF (2000) *J Bacteriol* 182:5807–5812.
19. Conway AB, Lynch TW, Zhang Y, Fortin GS, Fung CW, Symington LS, Rice PA (2004) *Nat Struct Mol Biol* 11:791–796.
20. Kim CA, Phillips ML, Kim W, Gingery M, Tran HH, Robinson MA, Faham S, Bowie JU (2001) *EMBO J* 20:4173–4182.
21. Biswas T, Aihara H, Radman-Livaja M, Filman D, Landy A, Ellenberger T (2005) *Nature* 435:1059–1066.
22. Nunes-Duby SE, Matsumoto L, Landy A (1987) *Cell* 50:779–788.
23. Kitts PA, Nash HA (1988) *J Mol Biol* 204:95–107.
24. Lewis JA, Hatfull GF (2001) *Nucleic Acids Res* 29:2205–2216.
25. Yu A, Haggard-Ljungquist E (1993) *J Bacteriol* 175:7848–7855.
26. Esposito D, Scoeca JJ (1997) *J Biol Chem* 272:8660–8670.
27. Lewis JA, Hatfull GF (2003) *J Mol Biol* 326:805–821.
28. Abbani M, Iwahara M, Clubb RT (2005) *J Mol Biol* 347:11–25.
29. Esposito D, Scoeca JJ (1994) *Mol Microbiol* 13:685–695.
30. Eriksson JM, Haggard-Ljungquist E (2000) *J Bacteriol* 182:6714–6723.
31. Connolly KM, Iwahara M, Clubb RT (2002) *J Bacteriol* 184:2088–2099.
32. Rudy CK, Scott JR, Churchward G (1997) *J Bacteriol* 179:2567–2572.
33. West SC (2003) *Nat Rev Mol Cell Biol* 4:435–445.
34. Erzberger JP, Mott ML, Berger JM (2006) *Nat Struct Mol Biol* 13:676–683.
35. Dame RT (2005) *Mol Microbiol* 56:858–870.
36. Luijsterburg MS, Noom MC, Wuite GJ, Dame RT (2006) *J Struct Biol* 156:262–272.
37. Story RM, Weber IT, Steitz TA (1992) *Nature* 355:318–325.
38. Sanders ER, Johnson RC (2004) *J Mol Biol* 340:753–766.
39. Dhar G, Sanders ER, Johnson RC (2004) *Cell* 119:33–45.
40. Yin S, Bushman W, Landy A (1985) *Proc Natl Acad Sci USA* 82:1040–1044.